Conformation and quantum-interference-enhanced thermoelectric properties of diphenyl-diketopyrrolopyrrole (DPP) derivatives.

Renad Almughathawi[1], Songjun Hou[1], Qingqing Wu[1]*, Zitong Liu[2], Wenjing Hong[3], and Colin Lambert[1]*

[1]Physics Department, Lancaster University, LA1 4YB Lancaster, United Kingdom

[2]Beijing National Laboratory for Molecular Sciences, CAS Key Laboratory of Organic Solids, Institute of Chemistry, Chinese Academy of Sciences, Beijing 100190, China

[3]State Key Laboratory of Physical Chemistry of Solid Surfaces, iChEM, NEL, College of Chemistry and Chemical Engineering, Xiamen University, Xiamen 361005, China

Supporting Information Placeholder

ABSTRACT: Manipulating the connectivity of external electrodes to central rings of carbon-based molecules in single molecule junctions is an effective route to tune their thermoelectrical properties. Here we investigate the connectivity dependence of the thermoelectric properties of a series of thiophene-DPP derivative molecules using density functional theory and tight-binding modelling, combined with quantum transport theory. We find a significant dependence of electrical conductance on the connectivity of the two thiophene rings attached to the DPP core. Interestingly, for connectivities corresponding to constructive quantum interference (CQI) different isomers obtained by rotating the thiophene rings possess the same electrical conductance while those corresponding to destructive quantum interference (DQI) show huge conductance variations upon ring rotation. Furthermore, we find that DQI connectivity leads to enhanced Seebeck coefficients, which can reach $500\sim700\ \mu V/K$. After including the contribution to the thermal conductance from phonons, the full figure of merit ZT for the CQI molecules could reach 1.5 at room temperature and it would further increase to 2 when temperature elevates to $400K$. Finally, we demonstrate that doping with tetracyanoquinodimethane (TCNQ) can change the sign of the Seebeck coefficients by forming a charge transfer system with the DPP.

KEYWORDS: molecular electronics, diketopyrrolopyrrole (DPP) derivatives, quantum interference, thermoelectric properties, charge-transfer complex

The foundational experiments of Nongjian Tao[1] and subsequent work exploring charge transport through single molecules connected to two metallic electrodes[2,3,4] has led to the design of molecular-scale components such as switches[4,5,6], rectifiers[7], and highly conjugated molecular wires[8]. A more recent goal of this research is the design of thermoelectric materials[9] or devices[10] based on single molecules or self-assembled monolayers[11], which can convert heat into electricity and contribute to the global challenge of green energy harvesting. Such organic materials and devices are potentially light-weight, flexible, environmentally friendly and cost-effective[12,13]. Diphenyl- DPP discovered by Farnum et al. in 1974[14] has unique properties, such as good conjugation, the strong electron-withdrawing ability, thermal and photostability, and the high fluorescence quantum efficiency[15,16]. It is widely used as a building block for organic molecules, both for fundamental studies of electronic properties and for industrial applications as dyes and pigments[15,17]. Furthermore, the DPP-based molecule could be placed between aromatic rings such as the five-membered heterocycle thiophene,[18] which creates the possibility of tuning their transport properties. In this paper, stimulated by measurements of thermoelectricity in bulk DPP-based films, which show that a thermoelectric figure of merit of $ZT = 0.25$ could be achieved,[19] we examine how room-temperature quantum interference in DPP cores influences their charge and heat transport properties and assess whether or not DPP derivatives are potential thermoelectric materials at the nanoscale.

Figure 1a shows the series of molecules of interest. DPP1, DPP2 and DPP3 contain thiophene rings with different connectivities, corresponding to inequivalent positions of the sulphur atoms of the thiophenes. Furthermore, each molecule is found to have two stable geometries labelled a or b, corresponding to different orientations of the thiophene rings relative to the DPP core. In what follows, we shall show that the Seebeck coefficients of DPP2 and DPP3 could reach $500-700\ \mu$V/K. After including the contribution of phonons to the thermal conductance, the full ZT for molecules DPP1-a and -b reach 1.5 at room temperature and it could increase to 2 when the temperature increases to $400K$. By exploring the effect of charge-transfer doping using tetracyanoquinodimethane (TCNQ), which is a well-known electron acceptor[20,21], we found that TCNQ can be used to change the sign change of the Seebeck coefficients.

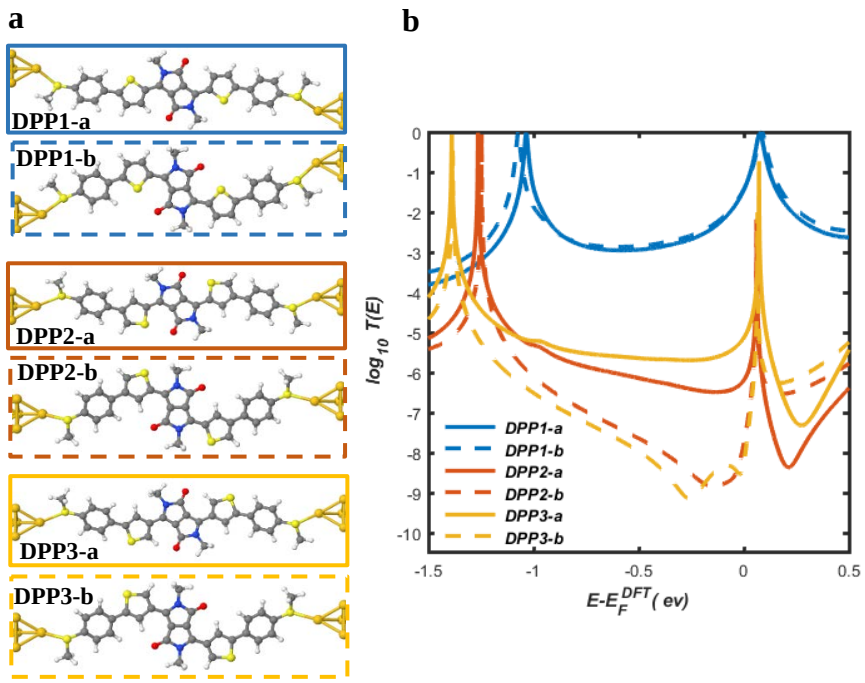

Figure 1. **Charge transport properties of diketopyrrolopyrrole (DPP) derivative isomers attached to gold electrodes via -SMe anchor groups.** (a) Models of the gold/molecule/gold sandwich junctions. The colors assigned to the atoms are as follows: grey for carbon, yellow for sulphur, red for oxygen, blue for nitrogen, white for hydrogen and orange for gold electrode atoms. (b) DFT-based transmission spectra against Fermi energy (E_F) in units of the quantum conductance $G_0 = 77\mu S$. DPP1-a, b (blue solid and dashed curves) exhibit constructive quantum interference (CQI) while DPP2-a, b (red solid and dashed curves) and DPP3-a, b (yellow solid and dashed curves) display destructive quantum interference (DQI).

Results and discussion

We systematically investigated the electrical and thermoelectrical properties of gold/ thiophene-diketopyrrolopyrrole (DPP) /gold hybrid junctions (figure 1a) using quantum transport theory combined with the mean-field Hamiltonian of each geometry obtained from tight-binding binding models of each molecule (see more details in Methods). The DPP derivative isomers are defined through their connectivity and orientation of the thiophene rings. To reveal the effect of these features on transport properties, the a and b contact geometries between electrodes and molecules were fixed, and therefore the b geometry is obtained by rotating the linkers and the electrodes of a relative to the DPP-core by 180° degrees around the molecule axis. We find the b isomers display very similar transmission functions before and after their geometrical relaxation (See figures S1, S2 of SI). Figure 1b shows that both DPP1-a and DPP1-b exhibit CQI, signaled by the absence of a dip in their transmission functions $T(E)$ within the HOMO-LUMO gap, whereas both isomers of DPP2 and DPP3 exhibit DQI signaled by the presence of such a dip. In all cases, charge transport is mainly LUMO-dominated.

It is interesting to note quantum interference is sensitive to the dihedral angle between the central core and the neighbouring thiophenes. To demonstrate this effect, we performed calculations, in which the two electrode-anchor-phenyl-thiophene sub-structures are rotated through a dihedral angle θ, as indicated in the figure S8. Taking DPP2 as an example, figures S8 (b) and (c) show the total energy against dihedral angle θ and the corresponding transmission spectra arising for different values of θ. The two configurations (0° (DPP2-b) and 180° (DPP2-a)) have lower energies. The former is a global minimum and the latter is a local minimum. By increasing θ from 0° (DPP2-b) to 180° (DPP2-a), the destructive quantum interference dip first moves to right and then moves back. Therefore, the quantum interference pattern is indeed sensitive to rotations, with the mid-gap transmission decreasing by almost four orders of magnitude at the most energetically unfavourable angles. Rotation-angle sensitivities of this kind have been reported for other molecules in the literature, examples of which can be found in[31,32].

The transmission functions of molecules DPP1-a, DPP1-b, which exhibit CQI (the blue solid and dashed curves) are rather similar. In contrast, the different isomers of molecules exhibiting DQI possess significantly different transmission functions. Near their transmission minima, the transmission coefficients of DPP2-a and DPP3-a (red and orange solid curves) are two to three orders of magnitude higher than those of DPP2-b and DPP3-b (red and orange dashed curves). These features in transmission functions could be interpreted from the perspective of the quantum interference between the molecular orbitals. From the molecular orbitals (MOs) of the gas-phase molecules DPP1, 2 and 3, Table S3 of the SI shows that the frontier molecular orbitals of DPP1-a, b are delocalized across the molecule, while for DPP2-a, b and DPP3-a, b, the LUMO is localized on the DPP core. Consequently, the LUMO of these molecules will not contribute significantly to the transmission function. Furthermore, from the phases of the MOs on the terminal groups, it is clear that the LUMO+1 and HOMO will interfere destructively according to orbital product rule[22,23]. In contrast, the delocalized LUMO of DPP1 interferes constructively with the HOMO, which leads to the higher transmission around Fermi energy. As indicated by the arrows in Tables S1 and S2, the LUMOs of DPP2-a and DPP3-a have a larger weight on the terminal groups than those of DPP2-b and DPP3-b, which contributes to the higher transmission coefficient within the HOMO-LUMO gap of DPP2, 3-a compared with DPP2, 3-b, shown in figure 1.

The difference between transmission functions of molecules exhibiting CQI or DQI is mainly attributed to the connectivity of the thi-

ophene rings. In order to illustrate the dependence of the connectivity on transmission coefficients, it is helpful to understand the properties of central cores formed from thiophene rings alone. Figures 2a and 2c show the transmission functions of cores formed from thiophene monomers and thiophene dimers with different connectivities. The transmission functions of molecules S2, S2', S3, S3' in figure 2b and 2d (red and yellow curves) exhibit DQI signalled by the presence of a dip in the $T(E)$ within the HOMO-LUMO gap, whereas those of molecules S1 and S1' in figure 2b and 2d (blue curves) exhibit CQI, signalled by the absence of such a dip. The qualitative features of this connectivity dependence is captured by a simple tight-binding models (TBM), in which the π orbitals are assigned nearest neighbour couplings only. Figure S3 of the SI shows the numbering system used to label atoms in these models.

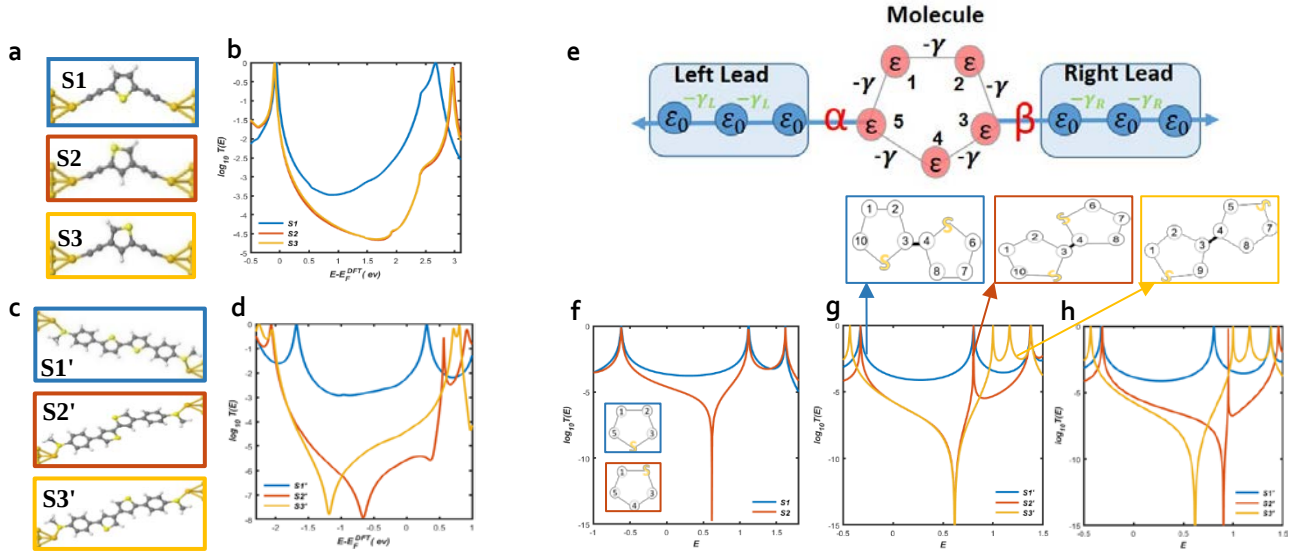

Figure 2. **Comparison of DFT and tight-binding model-based transmission functions for three different connectivities of monomer and dimer thiophene rings.** (a) Junctions formed from thiophene monomers **S1, S2, S3** with different connectivities. (b) The corresponding DFT-based transmission coefficients. (c) Junctions formed from thiophene dimers **S1', S2', S3'** with the connectivities corresponding to those of molecules DPP1-a, DPP2-a and DPP3-a in figure1a. (d) The corresponding DFT-based transmission coefficients. (e) A tight-binding model (TBM) consisting of a five-membered ring attached to two semi-infinite one-dimensional chains through weak couplings $\alpha = \beta = 0.1$. The on-site energies of the molecule (red dots) and the leads (blue dots) are ε and ε_0 respectively. In the simplest model considered here, these are all set to zero except for those sites occupied by sulphur (see Methods), which are assigned an on-site energy ϵ_s. For **S1**, **S2** and **S3**, the sulphur sites are 4, 1 and 2 respectively and the leads are connected to sites 3 and 5. The hopping integrals between nearest neighbour atoms are set to $-\gamma = -\gamma_L = -\gamma_R = -1$. (f) TBM transmission functions for **S1** and **S2**, obtained with a sulphur on-site energy of $\epsilon_s = -2$. By symmetry, the transmission function of **S3** is identical to that of **S2**. (g) TBM transmission functions for two thiophene rings with sites (10, 6) and (1, 7) connected to one-dimensional leads respectively. The TB lattices associated with each curve are indicated by blue red and yellow arrows and correspond to the connections to the cores of S1' to S3' shown in 2(c). For each connectivity, the on-site energies of both sulphurs have the same value ($\epsilon_s = -2$). (h) As for figure g, except the on-site energies of both sulphurs of **S2'** are changed to $\epsilon_s = -1.2$, to account for the fact that their environments differ from those of **S1'**. This moves the curves closer to DFT results shown in figure 2d.

The values used for the site energies of the sulphurs in the tight binding model of figures 2f and 2h are guided by our DFT calculations. Comparison between the two approaches show that a TBM with only a single free parameter (ie the sulphur site energy ϵ_s) can capture the main qualitative features of the much more demanding DFT simulations. To illustrate the role of this parameter, figure S3 shows how the TBM transmission coefficients would change if other non-optimal values of ϵ_s are chosen. Results are shown for a series of on-site energies of the sulphurs, ranging from $\epsilon_s = -0.4$ to $\epsilon_s = -2$ and reveal that the transmission dip moves to lower energies as ϵ_s becomes more negative.

Starting from the DFT-based transmission functions, we evaluated thermoelectric properties of the above molecules (see Methods), including their electrical conductances G, their Seebeck coefficients S, electronic thermal conductances κ_e and electronic figure of merit ZT_e. These are shown in figure 3. The Mott formula $S \propto -\frac{\partial lnT(E)}{\partial E}|_{E=E_F}$ indicates that a large Seebeck coefficient can be obtained if the Fermi energy (E_F) happens to coincide with a steep slope of electron transmission coefficient T(E)[24,25]. As a consequence, the Seebeck coefficient is higher for molecules exhibiting DQI (red yellow curves) as shown in figure 3b. We find that the Seebeck coefficients for DQI molecules DPP2-a, 2-b and DPP3-a, 3-b could reach $400\sim700\ \mu V/K$. Figure 3c shows the thermal conductance κ_e due to the electrons obtained from the electron transmission functions (see Methods). The heat transport due to electrons for the CQI in figure 3c (blue curve) has the similar shape to CQI of the electrical conductance in figure 3a, reflecting the Wiedemann-Franz law. The thermal conductance due to electrons for DPP1-a and 1-b is in the range between $1\sim40\ pW/K$ which is comparable with typical thermal conductances due to phonons $\sim10\ pW/K$. The molecules exhibiting DQI possess substantially lower values of κ_e. Consequently, their high electronic figures of merit ZT_e do not lead to high values of the full ZT.

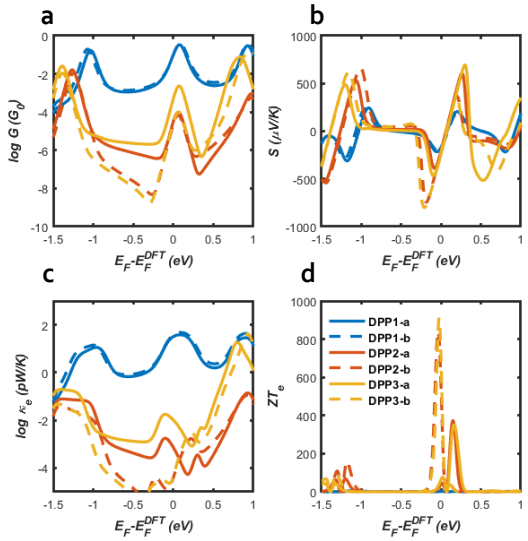

Figure 3. **Thermoelectric properties of the thiophene-DPP isomers as the function of the Fermi energy at room temperature 300K**. (a) Electrical conductance $G(E_F)$. (b) Seebeck coefficients$S(E_F)$. (c) Thermal conductance $\kappa_e(E_F)$. (d) Electronic figure of merit $ZT_e(E_F)$.

Figure 4 shows the effect of temperature (T) on the thermoelectric performance of thiophene-DPP derivatives and reveals that $\mathrm{ZT}_e(T)$ increases with temperature up to a maximum value, before decreasing at higher temperatures. As mentioned above, the electronic figure of merit $\mathrm{ZT}_e(T)$ only includes the thermal conductance κ_e.

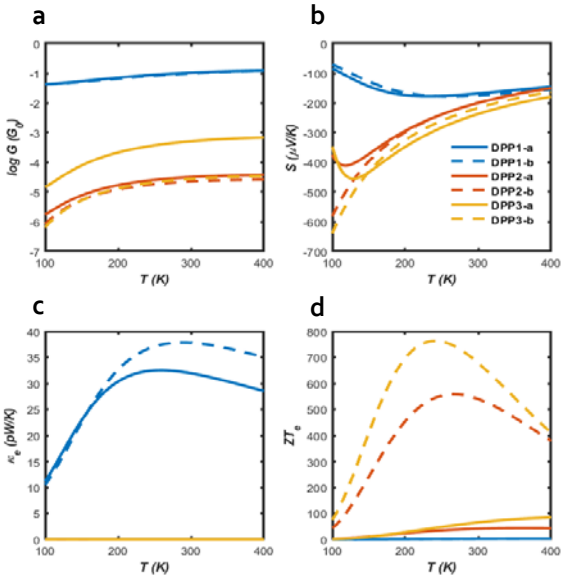

Figure 4. **Thermoelectric properties of the molecules as a function of temperature at $E_F = 0$ eV:** (a) Electrical conductance *G(T).* (b) Seebeck coefficients $S(T)$. (c) Thermal conductance κ_e. (d) Electronic figure of merit $\mathrm{ZT}_e(T)$.

When the thermal conductance due to the phonons κ_{ph} is included[26], the full $ZT = S^2GT/(\kappa_e + \kappa_{ph})$ [27] and only this is physically relevant. In order to compute the phonon contribution κ_{ph} to the thermal conductance, we calculate the transmission coefficient of phonon $T_{ph}(\hbar\omega)$ as a function of their frequency ω (see Methods). Since the highest ZT occurs when κ_{ph} is less than or comparable with κ_e, we focus initially on the highest conductance molecule DPP1-a, whose the phonon transmission coefficient and the thermal conductance due to the phonons are presented in figures 5a and b. The phonon thermal conductances are found to be $16.9\,pW/K$ and $8\,pW/K$ for DPP2-a and DPP2-b respectively (see figure S6 of SI). For DPP1-a figure 5c shows the room-temperature full ZT versus the Fermi-energy and demonstrates a high room-temperature $ZT \sim 1.5$ is achievable. Figure 5d shows the temperature dependence of ZT for all molecules and reveals that the ZT of DPP1 can reach ~ 2 when the temperature increases to $400K$. However, the molecules exhibiting DQI show quite low values of the full ZT, because that the phonon thermal conductance k_{ph} dominates the electronic contribution. DPP2/3-b have the lowest electrical conductances and the highest Seebeck coefficients. The electronic figure of merit is $ZT_e = GS^2T/\kappa_e$ and therefore, if phonons are neglected and provided the Wiedemann-Franz law is valid (ie $\frac{G}{\kappa_e} = \text{constant}$), the molecules with the highest S will have the highest ZT_e. However this means that the low-G molecules have low values of κ_e and therefore after including the phonons the percentage increase in thermal conductance is greatest for low-G molecules. This is why molecules with high ZT_e have a low ZT . More quantitatively, the thermal conductance due to phonons is of order $\kappa_{ph} = 8pW/K$, whereas for the low-G molecules DPP2-b and DPP3-b, $\kappa_e \approx 10^{-4}pW/K$. Consequently, phonons dominate their thermal conductance and their full ZT is low. For the CQI molecules DPP1-a/b where $\kappa_{ph} = 11pW/K$ and $\kappa_e = 32pW/K$, the full ZT is higher, because phonons have a much smaller effect on the thermal conductance.

Figure S5 of the SI shows that a similar temperature dependence is obtained if the Fermi energy deviates from the DFT-predicted value by -0.1eV.

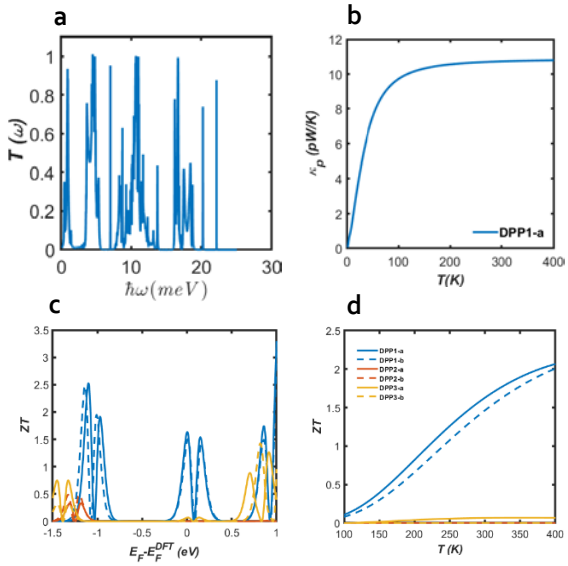

Figure 5. **Thermoelectric properties of the molecules** (a) Phonon transmission function for DPP1-a. (b) Phononic contribution to the thermal conductance for DPP1-a. (c) Full ZT as a function of Fermi energy at room temperature $300\ K$ for molecules shown in figure 1a. (d) Full ZT as a function of temperature for molecules shown in figure 1a.

Starting from the above molecular junctions, we consider the possibility of tuning their electrical and thermoelectrical properties, by doping with TCNQ[21,28] to form charge-transfer complexes. Our aim is to investigate the influence of the presence of TCNQ acceptor

molecule on the transmission coefficient of the DPP derivatives in figure 1a. As an example, we chose DPP-1, because the un-doped molecule has the highest T. Starting from this high value, the aim is to determine if it possible to increase ZT even further. DPP-1a and DPP1-b have the same central core and will bind to TCNQ in the manner. The results in figure 6b show that TCNQ gains electrons from the backbone, which induces negative gating on the backbone DPP1-b. Consequently, spin polarised transport is observed due to the charge transfer from the DPP1-b to TCNQ. In addition, the two Fano-resonances are generated due to the weak coupling between the acceptor and donor, so that the acceptor behaves like a pendant group[29,30]. Then, if we replaced sulphur atom with oxygen, there is no significant difference in the behaviour of the transmission coefficient (figure S7). For the DPP1-b+TCNQ complex, we computed the thermoelectric properties, the electrical conductance, the Seebeck coefficient and the full ZT by using an estimated k_{ph} value equal to 10 PWK^{-1}. In the range between the two vertical dashed lines in figure 6d, the Seebeck coefficients are positive, which indicates that the sign is tuned by TCNQ doping. The full ZT is around 0.1 which is suppressed compared to the un-doped junction.

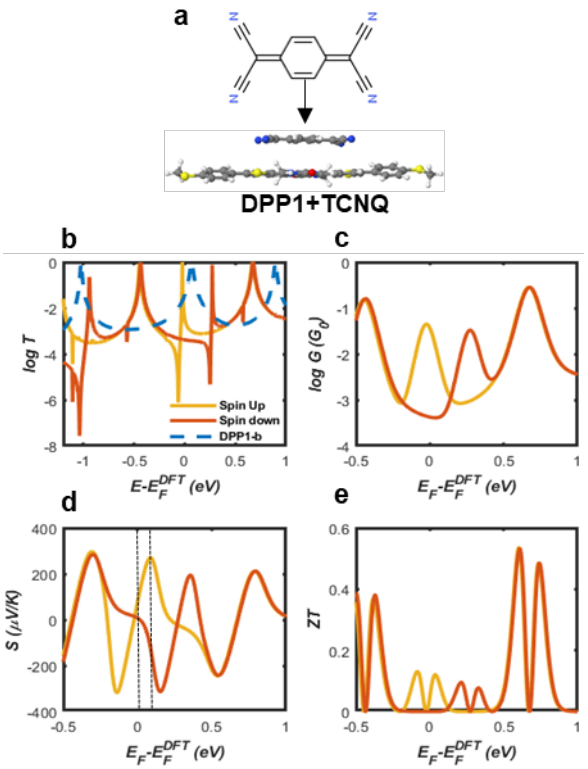

Figure 6. **DFT-based transmission functions for DPP1-b+TCNQ. (**a) Configuration of the system containing a single molecule DPP1 with TCNQ. (b) Transmission coefficients against Fermi energy E_F. Blue curve represents the transmission functions of DPP1-b while red and yellow curves depict the spin up and spin down transmission functions of the donor-acceptor charge-transfer complex respectively. (c) Electrical conductance G. (d) Seebeck coefficients S. (e) Room-temperature ZT versus Fermi energy.

Conclusion

Based on density functional theory and the quantum transport theory, the electron transport properties have been investigated for thiophene-DPP derivatives (DPP1, DPP2 and DPP3). This work illustrates that varying the position of the sulphur atom in thiophene rings has a significant influence on their electrical and thermoelectric properties. It is further verified by studying the connectivity of the two-thiophene-ring systems in the absence of DPP-core. In addition, the rotation of the flanked rings could cause huge variations in the conductance when inserting the DPP core into the two-thiophene system. Furthermore, DQI molecules 2 and 3 systems show high Seebeck coefficients, which could reach $500\sim700\ \mu V/K$. After including the contribution from phonons to the thermal conductance, we found that due to the presence of CQI, the full ZT of DPP1 reaches 1.5 at room-temperature and it could increase to 2 when temperature elevates to 400K. Finally, we demonstrated that the Seebeck could be further tuned by introducing a TCNQ dopant which could gain electrons from DPP, leading to the sign change for the Seebeck coefficients even though DPP is a stronger acceptor. These results suggest that DPP derivatives are versatile materials for thermoelectric functions, whose performance can be tuned by varying their connectivity to electrodes, changing the positions of sulphur atoms and varying the orientation of their thiophene rings to obtain different isomers.

Methods

DFT calculation:

The optimized geometry and ground state Hamiltonian and overlap matrix elements of each structure was self-consistently obtained using the SIESTA[33] implementation of density functional theory (DFT). SIESTA employs norm-conserving pseudo-potentials to account for the core electrons and linear combinations of atomic orbitals to construct the valence states. The generalized gradient approximation (GGA) of the exchange and correlation functional is used with the Perdew-Burke-Ernzerhof parameterization (PBE)[34] a double-ζ polarized (DZP) basis set, a real-space grid defined with an equivalent energy cut-off of 200 Ry. The geometry optimization for each structure is performed to the forces smaller than 10 meV/Ang.

Tight-Binding Model:

The Hamiltonian of the simple tight-binding model describes a single orbital per atom with nearest-neighbour couplings $\gamma = -1$. All site energies are set to zero, except the site energies of sulphurs, which in figure S3 were chosen to range from -0.4 to -2.

Transport calculations:

The mean-field Hamiltonian obtained from the converged DFT calculation or a tight-binding Hamiltonian (using single orbital energy site per atom with Hückel parameterisation) was combined with our home-made implementation Gollum[35] to calculate the phase-coherent, elastic scattering properties of each system consisting of left gold (source) and right gold (drain) leads and the scattering region (molecule DPP1, DPP2, DPP3). The transmission coefficient $T(E)$ for electrons of energy E (passing from the source to the drain) is calculated via the relation:

$$T(E) = Trace\left(\Gamma_R(E)G^R(E)\Gamma_L(E)G^{R\dagger}(E)\right) \quad (1)$$

In this expression, $\Gamma_{L,R}(E) = i\left(\Sigma_{L,R}(E) - {\Sigma_{L,R}}^{\dagger}(E)\right)$ describe the level broadening due to the coupling between left (L) and right (R) electrodes and the central scattering region, $\Sigma_{L,R}(E)$ are the retarded self-energies associated with this coupling and $G^R(E) = (ES - H - \Sigma_L - \Sigma_R)^{-1}$ is the retarded Green's function, where H is the Hamiltonian and S is overlap matrix. Using obtained transmission coefficient $T(E)$, the electrical conductance G, the Seebeck coefficient S and the thermal power GS^2 can be calculated through the following formula:

$$G = G_0\, L_0 \tag{2}$$

$$S = -\frac{L_1}{|e|TL_0} \tag{3}$$

$$\kappa_e = -2\frac{L_0L_2 - {L_1}^2}{hTL_0} \tag{4}$$

$$ZT_e = \frac{{L_1}^2}{L_0L_2 - {L_1}^2} \tag{5}$$

In the linear response the quantity of Lorenz number $L_n(\mathrm{T}, E_F)$ is giving by

$$L_n(\mathrm{T}, E_F) = \int_{-\infty}^{+\infty} dE(E - E_F)^n\, \mathrm{T(E)} \left(-\frac{\partial f(E)}{\partial E}\right) \tag{6}$$

Where $G_0 = 2e^2/h$ is conductance quantum, e is the charge of an electron; h is the Planck's constant; E_F is the Fermi energy; $f(E) = (1 + exp((E - E_F)/k_BT))^{-1}$ is the Fermi–Dirac distribution function, T is the temperature, and $k_B = 8.6 \times 10^{-5}$ eV/K is Boltzmann's constant.The electronic figure of merit ignores the thermal conductance k_{ph} due to phonons, whereas the figure of merit ZT experimentally is defined by $ZT = S^2GT/(k_e + k_{ph})$, which includes the thermal conductance due to both phonons and electrons in the denominator. To calculate the thermal conductance k_{ph} due to phonons, the force constant matrix, K is obtained by finite differences:

$$K_{i\alpha,j\beta} = \frac{\partial^2 E}{\partial r_{i\alpha}\partial r_{j\beta}} = -\frac{F_{j\beta}(Q_{i\alpha}) - F_{j\beta}(-Q_{i\alpha})}{2Q_{i\alpha}} \tag{7}$$

Where E is the total energy and $r_{i\alpha}(r_{j\beta})$ is the displacement of atom $i(j)$ in the coordinate direction $\alpha(\beta)$. The geometry is relaxed until the force of each atom is equal to 0.01 eV Å^{-1}. By shifting each atom (i) with $Q_{i\alpha} = \pm 0.01\ A^{\circ}$ in the direction $\alpha = x, y, z$ the forces on atom along $\beta = x, y, z$ direction, where $F_{j\beta}(Q_{i\alpha})$ is calculated. Thus, the dynamical matrix D can be obtained by $D_{i\alpha,j\beta}/\sqrt{m_i m_j}$, where $m_i\, m_j$ are the mass of the atom i and atom j. Then the dynamical matrix is used to compute the transmission probability of phonons using Gollum transport code with eqn (1). The corresponding phonon thermal conductance is given by

$$k_{ph}(T) = \int_0^{\infty} \frac{\hbar\omega}{2\pi} T_{ph}(\omega) \frac{\partial f_{BE}(\omega,T)}{\partial T} d\omega \tag{8}$$

Where $\partial f_{BE}(\omega, T) = 1/[e^{\left(\frac{\hbar\omega}{K_BT}\right)} - 1]$ is the Bose–Einstein distribution.

ASSOCIATED CONTENT

Supporting Information

The Supporting Information is available free of charge on the ACS Publications website.

Details of DPP rotation geometries; thiophene connectivity; molecular orbital; charge transport properties; tight-binding model with more energies site; thermoelectric properties calculation of molecular junctions. (PDF)

AUTHOR INFORMATION

Corresponding Author

Qingqing Wu- Physics department, Lancaster University, LA1 4YB Lancaster, United Kingdom;

Email: q.wu6@lancaster.ac.uk

Colin Lambert - Physics department, Lancaster University, LA1 4YB Lancaster, United Kingdom;

Email: c.lambert@lancaster.ac.uk

Notes

The authors declare no competing financial interests.
Any additional relevant notes should be placed here.

ACKNOWLEDGMENT

Support from the UK EPSRC is acknowledged, through grant nos. EP/N017188/1, EP/M014452/1, EP/P027156/1 and EP/N03337X/1. Support from the European Commission is provided by the FET Open project 767187 – QuIET. R. Almughathawi acknowledges the ministry of education Saudi Arabia, and Taibah University.

REFERENCES

(1) Xu, Bingqian, N. T. Single-Molecule Resistance Measured by Repeated Formation of Molecular Junctions. *Science.* **2003**, *301*, 1221–1223.

(2) Sendler, T.; Luka-Guth, K.; Wieser, M.; Lokamani; Wolf, J.; Helm, M.; Gemming, S.; Kerbusch, J.; Scheer, E.; Huhn, T.; Erbe, A. Light-Induced Switching of Tunable Single-Molecule Junctions. *Adv. Sci.* **2015**, 2, 1500017.

(3) Lambert, C. Basic Concepts of Quantum Interference and Electron Transport in Single-Molecule Electronics. *Chem. Soc. Rev.* **2015**, *44* (4), 875–888.

(4) Wu, Q.; Hou, S.; Sadeghi, H.; Lambert, C. A Single-Molecule Porphyrin-Based Switch for Graphene Nano-Gaps. *Nanoscale* **2018**, *10*, 6524–6530.

(5) Moresco, F.; Meyer, G.; Rieder, K.-H.; Tang, H.; Gourdon, A.; Joachim, C. Conformational Changes of Single Molecules Induced by Scanning Tunneling Microscopy Manipulation: A Route to Molecular Switching. *Phys. Rev. Lett.* **2001**, *86* (4), 672-675.

(6) Kronemeijer, A. J.; Akkerman, H. B.; Kudernac, T.; van Wees, B. J.; Feringa, B. L.; Blom, P. W. M.; de Boer, B. Reversible Conductance Switching in Molecular Devices. *Adv. Mater.* **2008**, *20* (8), 1467–1473.

(7) Aviram, A.; Ratner, M. A. Molecular Rectifiers. *Chem. Phys. Lett.* **1974**, *29* (2), 277–283.

(8) Xu, W.; Leary, E.; Hou, S.; Sangtarash, S.; González, M. T.; Rubio-Bollinger, G.; Wu, Q.; Sadeghi, H.; Tejerina, L.; Christensen, K. E.; Agraït, N.; Higgins, S. J.; Lambert, C. J.; Nichols, R. J.; Anderson, H. L. Unusual Length Dependence of the Conductance in Cumulene Molecular Wires. *Angew. Chemie* **2019**, 58, 8378–8382.

(9) Hou, S.; Wu, Q.; Sadeghi, H.; Lambert, C. J. Thermoelectric Properties of Oligoglycine Molecular Wires. *Nanoscale* **2019**, *11* (8), 3567–3573.

(10) Wu, Q.; Sadeghi, H.; García-Suárez, V. M.; Ferrer, J.; Lambert, C. J. Thermoelectricity in Vertical Graphene-

C60-Graphene Architectures. *Sci. Rep*. **2017**, 7, 11680.

(11) Ismael, A.; Wang, X.; Bennett, T. L.; Wilkinson, L. A.; Robinson, B. J.; Long, N. J.; Cohen, L. F.; Lambert, C. J. Tuning the Thermoelectrical Properties of Anthracene-Based Self-Assembled Monolayers. *Chem. Sci.* **2020**, 11, 6836–6841.

(12) Zhang, Q.; Sun, Y.; Xu, W.; Zhu, D. Organic Thermoelectric Materials: Emerging Green Energy Materials Converting Heat to Electricity Directly and Efficiently. *Adv. Mater.* **2014**, *26* (40), 6829–6851.

(13) Malen, J. A.; Yee, S. K.; Majumdar, A.; Segalman, R. A. Fundamentals of Energy Transport, Energy Conversion, and Thermal Properties in Organic-Inorganic Heterojunctions. *Chem. Phys. Lett.* **201**0, 491, 109–122.

(14) Farnum, D. G.; Mehta, G.; Moore, G. G. I.; Siegal, F. P. Attempted Reformatskii Reaction of Benzonitrile, 1,4-Diketo-3,6-Diphenylpyrrolo[3,4-C]Pyrrole. A Lactam Analogue of Pentalene. *Tetrahedron Lett.* **1974**, 29, 2549–2552.

(15) Grzybowski, M.; Gryko, D. T. Diketopyrrolopyrroles: Synthesis, Reactivity, and Optical Properties. *Adv. Opt. Mater.* **2015**, 3, 280–320.

(16) Wang, X.; Jiang, B.; Du, C.; Ren, X.; Duan, Z.; Wang, H. Fluorinated Dithienyl-Diketopyrrolopyrrole: A New Building Block for Organic Optoelectronic Materials. *New J. Chem.* **2019**, 43, 16411–16420.

(17) Liu, Q.; Bottle, S. E.; Sonar, P. Developments of Diketopyrrolopyrrole-Dye-Based Organic Semiconductors for a Wide Range of Applications in Electronics. *Adv. Mater*. 2020, 32, 1903882.

(18) Wang, Z.; Liu, Z.; Ning, L.; Xiao, M.; Yi, Y.; Cai, Z.; Sadhanala, A.; Zhang, G.; Chen, W.; Sirringhaus, H.; Zhang, D. Charge Mobility Enhancement for Conjugated DPP-Selenophene Polymer by Simply Replacing One Bulky Branching Alkyl Chain with Linear One at Each DPP Unit. *Chem. Mater.* **2018**, *30* (9), 3090–3100.

(19) Ding, J.; Liu, Z.; Zhao, W.; Jin, W.; Xiang, L.; Wang, Z.; Zeng, Y.; Zou, Y.; Zhang, F.; Yi, Y.; Diao, Y.; McNeill, C. R.; Di, C. an; Zhang, D.; Zhu, D. Selenium-Substituted Diketopyrrolopyrrole Polymer for High-Performance p-Type Organic Thermoelectric Materials. *Angew. Chemie - Int. Ed.* **2019**, *58* (52), 18994–18999.

(20) Acker, D. S.; Harder, R. J.; Hertler, W. R.; Mahler, W.; Melby, L. R.; Benson, R. E.; Mochel, W. E. 7,7,8,8-Tetracyanoquinodimethane and Its Electrically Conducting Anion-Radical Derivatives. *J. Am. Chem. Soc.* **1960**, 82 (24), 6408-6409.

(21) Herman, F.; Batra, I. P. Electronic Structure of the Tetracyanoquinodimethane (TCNQ) Molecule. *Phys. Rev. Lett.* **1974**, *33* (2), 94–97.

(22) Lambert, C. J.; Liu, S. X. A Magic Ratio Rule for Beginners: A Chemist's Guide to Quantum Interference in Molecules. *Chem. - A Eur. J.* **2018**, 24, 4193-4201.

(23) Yoshizawa, K.; Tada, T.; Staykov, A. Orbital Views of the Electron Transport in Molecular Devices. *J. Am. Chem. Soc.* **2008**, *130* (29), 9406–9413.

(24) Small, J. P.; Perez, K. M.; Kim, P. Modulation of Thermoelectric Power of Individual Carbon Nanotubes. *Phys. Rev. Lett.* **2003**, *91* (25), 1–4.

(25) Lunde, A. M.; Flensberg, K. On the Mott Formula for the Thermopower of Non-Interacting Electrons in Quantum Point Contacts. *J. Phys. Condens. Matter* **2005**, 17, 3879-3884.

(26) Bubnova, O.; Crispin, X. Towards Polymer-Based Organic Thermoelectric Generators. *Energy Environ. Sci.* **2012**,5, 9345–9362.

(27) Karamitaheri, H.; Pourfath, M.; Faez, R.; Kosina, H. Geometrical Effects on the Thermoelectric Properties of Ballistic Graphene Antidot Lattices. *J. Appl. Phys.* **2011**, *110* (5), 054506.

(28) Rudloff, M.; Ackermann, K.; Huth, M.; Jeschke, H. O.; Tomic, M.; Valentí, R.; Wolfram, B.; Bröring, M.; Bolte, M.; Chercka, D.; Baumgarten, M.; Müllen, K. Charge Transfer Tuning by Chemical Substitution and Uniaxial Pressure in the Organic Complex Tetramethoxypyrene-Tetracyanoquinodimethane. *Phys. Chem. Chem. Phys.* **2015**, *17* (6), 4118–4126.

(29) Wang, K.; Vezzoli, A.; Grace, I. M.; McLaughlin, M.; Nichols, R. J.; Xu, B.; Lambert, C. J.; Higgins, S. J. Charge Transfer Complexation Boosts Molecular Conductance through Fermi Level Pinning. *Chem. Sci.* **2019**, *10* (8), 2396–2403.

(30) Famili, M.; Grace, I. M.; Al-Galiby, Q.; Sadeghi, H.; Lambert, C. J. Toward High Thermoelectric Performance of Thiophene and Ethylenedioxythiophene (EDOT) Molecular Wires. *Adv. Funct. Mater.* **2018**, 28, 1703135.

(31) Venkataraman, L.; Klare, J. E.; Nuckolls, C.; Hybertsen, M. S.; Steigerwald, M. L. Dependence of Single-Molecule Junction Conductance on Molecular Conformation. *Nature* **2006**, 442, 904–907.

(32) Finch, C. M.; Sirichantaropass, S.; Bailey, S. W.; Grace, I. M.; García-Suárez, V. M.; Lambert, C. J. Conformation Dependence of Molecular Conductance: Chemistry versus Geometry. *J. Phys. Condens. Matter* **2008**, *20* (2), 022203.

(33) Soler, J. M.; Artacho, E.; Gale, J. D.; García, A.; Junquera, J.; Ordejón, P.; Sánchez-Portal, D. The SIESTA Method for Ab Initio Order-N Materials Simulation. *J. Phys. Condens. Matter* **2002**, 14, 2745–2779.

(34) Perdew, J. P.; Burke, K.; Ernzerhof, M. Generalized Gradient Approximation Made Simple. *Phys. Rev. Lett.* **1996**, *77* (18), 3865–3868.

(35) Ferrer, J.; Lambert, C. J.; Garcıa-Suárez, V. M.; Manrique, D. Z.; Visontai, D.; Oroszlany, L. R. Rodrıguez-Ferradá s, I. Grace, S. Bailey, and K. Gillemot. *New J. Phys* **2014**, *16*, 93029.

“For TOC only”

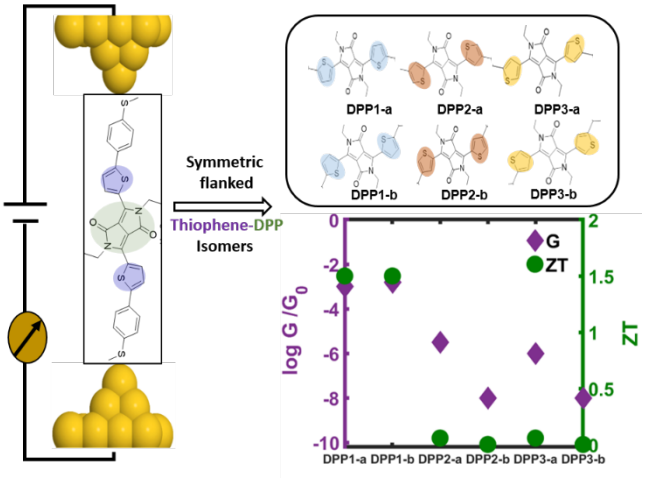
Symmetric
flanked
Thiophene-DPP
Isomers
DPP1-a
DPP2-a
DPP3-a
DPP1-b
DPP2-b
DPP3-b
G
ZT
log G /G0
ZT
0
-2
-4
-6
-8
-10
2
1.5
1
0.5
0
DPP1-a DPP1-b DPP2-a DPP2-b DPP3-a DPP3-b